Spatial Propagation Characteristics of 28 GHz Frequency Band in UMi Scenario

Yu Han, Lei Tian, Xinzhuang Zhang, Pan Tang, Zhixue Hu and Jianhua Zhang
Key Lab of Universal Wireless Communication, Ministry of Education
Beijing University of Post and Telecommunications, P.O.Box 92, Beijing 100876,China
Email:2015110446@bupt.edu.cn; tianlbupt@bupt.edu.cn; jhzhang@bupt.edu.cn

***Abstract*—This paper presents the wideband channel characteristics of 28 GHz in urban microcell (UMi) scenario based the measurement in Beijing. Both the omnidirectional-antenna-based measurement and the horn-antenna-based measurement are performed with bandwidth up to 800 MHz. The standard deviation of shadow fading (σ_{SF}) is studied and is compared with that value in standard protocol. Unlike traditional method, the σ_{SF} is calculated with data captured in each single route in this paper. It is found that in a specific environment, the standard model obtained by traditional method overestimate the σ_{SF} of this frequency band to a large extent both in line of sight (LOS) environment and non line of sight (NLOS) environment. In addition, the 3-Dimensional angle information is estimated with the space alternating generalized expectation-maximization (SAGE) algorithm. The angle spread of arrival (ASA) and the angle spread of departure (ASD) are investigated and the cluster characteristics at different rotation measurement sites are analysed. It is found that dimension of parameter space that used in clustering algorithm has a great impact on the clustering result of the recognizable multipaths.**

***Index Terms*—28 GHz, measurement, LOS, NLOS, σ_{SF}, ASA, ASD, clustering.**

I. Introduction

Nowadays, the rapidly rising demands for data transport calls for drastic improvement of the mobile network capacity. The millimeter wave (mmWave) that is ready to be used in the fifth generation (5G) communication system can help the implementation of high rate data transports. Successful deployment of mmWave mobile communication systems requires sufficient knowledge of the mmWave propagation channel [1]. So many measurement campaigns have been performed to study the characteristics of mmWave e.g. [2] [3] [4] [5]. The ITU-R Working Party 3K also established a new Correspondence Group CG-3K-6 to modify the Recommendations ITU-RP.1411 and P.1238 in the higher frequencies. This Group aims to progress the studies on mmWave as much as possible until the end of 2017.

The fundamental aspects of propagation characteristics of this new spectrum are the pathloss and shadow fading. Pathloss is the attenuation a signal experiences between transmitter and receiver (averaged over small-scale fading). It determines the range over which communication can take place, as well as the effect of interference. The shadow fading represents the random variation of signal amplitude caused by the obstacles or variation of reflector and scatterer in the propagation environment. The relevant study on pathloss and shadow fading of mmWave is rich e.g [4] [6]. The statistical-based empirical model combined the two parameters together to represent the above two phenomenon. However, [7] shows that pathloss models from traditional method can overestimate the signal variation. Because in traditional method, the measured data of different routes from one cell or from different cells are mingled. It is obvious that there is difference even between two same type environment and [9] has conformed the difference in coefficients of empirical pathloss model. In this paper, we will investigate the (σ_{SF}) at 28 GHz with the measured data in each single measured route instead of mingling the data from different routes together. We aim to study to what extend the traditional method overestimate the shadow fading both in the line-of-sight (LOS) and non-line-of-sight (NLOS) enviroments. Different obstacle size in the propagation environment will be considered when calculating the σ_{SF}. The result will be compared with the value in Recommendation [13].

In addition, enough knowledge of angular characteristics of the wideband mmWave channel is essential for the application of this spectrum and the propagation characteristics are related to specific environment to some extent. Therefore, this paper will study the 3-Dimensional angle characteristics of the 28 GHz wideband channel with data from rotation measurement at different sites for better understanding the propagation mechanism of signals in this spectrum. Both the angle of arrival (AOA) and angle of departure (AOD) in azimuth and elevation will be estimated with the SAGE algorithm [8], which removed the effect of antenna pattern. The azimuth angle spread of arrival (AASA), the elevation angle spread of arrival (EASA), the azimuth angle spread of departure (AASD) and the elevation angle spread of departure (EASD) will be investigated respectively.

Then the cluster characteristics will be studied based on the angle information. The clusters defined in standard model is calculated based on delay, AOA and AOD. However, it is very difficult to get the AOA and AOD simultaneous by rotation measurement. So in some papers like [11], the cluster is calculated only with the delay and AOA in azimuth and elevation while in paper [10] the cluster is estimated only with delay and AOD in azimuth and elevation. In this paper, both of the two methods will be used and the results will be compared to show the difference. We also compared the results with the value in standard Recommendation to show the influence of smaller dimension of the clustering algorithm parameter space

on clustering results.

II. Description of Measurement Campaign

The measurement campaign was performed in typical urban environment in Beijing with the mmWave channel sounder developed by National Instrument (NI) company. This equipment can show the real-time channel quality by very fast correlation. The signal bandwidth in this measurement is up to 800 MHz. The length of pseudo random sequence used in Transmitter (Tx) is 511. Fig. 1 shows the top view of the measurement scenario. Both LOS and NLOS routes are selected in this campaign. This measurement contains two parts: omnidirectional-antenna-based (OAB) measurement and horn-antenna-based (HAB) measurement.

A. Omnidirectional-antenna-based measurement

We used the omnidirectional antenna at receiver (Rx) and a sector antenna at Tx as shown in Fig. 2(b). The sector antenna that covers 120° in azimuth was used to increase the measurement range. For gathering enough data to investigate the shadow fading, the receiver moved along all the routes marked in red shown in Fig. 1 at a very low speed. Due to the heavy attenuation of this frequency band and the limited sensitivity of the measurement equipment, we did not get valid data in some NLOS routes.

B. Horn-antenna-based measurement

In the HAB measurement, a horn antenna was used and was placed on the antenna positioner which can rotate the antenna to any spatial direction in any step size as shown in Fig. 3(a). *Step 1:* Firstly, for obtaining the information of AOA, the horn antenna was used in the Rx and an omnidirectional antenna was used in the Tx. The rotation range and step size of the horn antenna are list in Rx section in table I. *Step 2:* Then we exchange the antennas in Tx and Rx. The omnidirectional antenna was place at the Rx. The horn antenna was placed in the Tx and was rotated according to the last line of table I for getting the information of AOD. Both in the two steps, the Rx was moved among the 13 sites marked with rhombus shown in Fig. 1 and the Tx was fixed. All the measured data in the 13 measured sites are valid.

III. Shadow Fading

In this section, the study of shadow fading is based on the measured data from OAB measurement. The channel impulse response (CIR) h which removed the antenna radiation pattern can be represented as

$$h = \sum_{i=1}^{I} \alpha_i e^{j\phi_i} \delta(\tau - \tau_i) \tag{1}$$

where α_i, ϕ_i and τ_i represent the amplitude response, phase, and the excess delay time of *i-th* delay signal. Then the attenuation at each measurement point can be calculated by

$$PL = -log10(\sum_{\tau} ||h(\tau)||^2) \tag{2}$$

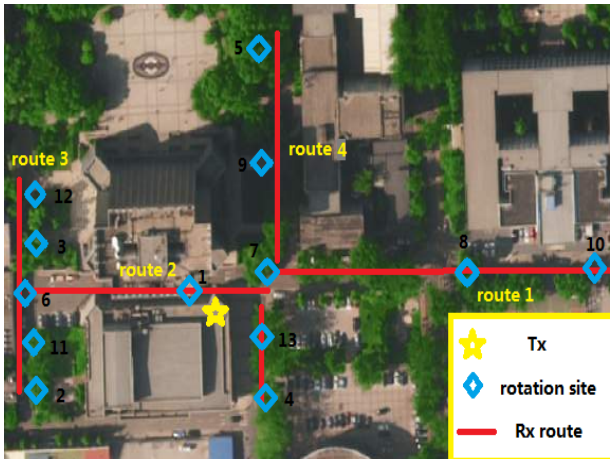

Fig. 1. Top view of scenario

(a) Tx (b) Rx

Fig. 2. The picture of Tx and Rx of the omnidirectional antenna based measurement

(a) Rx (b) Tx

Fig. 3. The picture of Tx and Rx of the rotated directional antenna based measurement

Empirical Statistical-based passloss models are normally represented as

$$PL(d)[dB] = PL_{intercept} + nlog10(d) + X_\sigma \tag{3}$$

where $PL_{intercept}$ and n are the intercept and slope. They can be obtained by linear fitting of the measured data. The X_σ reflects the effect of shadow fading. It describes the deviation of actual pathloss from the mean value. The standard deviation σ_{SF} of shadow fading can be calculated by

$$\sigma_{SF} = \sqrt{\frac{1}{N}\sum_{n=1}^{N}(PL_n - \mu_{PL})^2} \tag{4}$$

TABLE I
SPECIFICS OF THE ROTATED MEASUREMENT

		Range of azimuth	Range of elevation	Tx ∼ Rx distance [m]	Environment
Rx	1	$0^\circ \sim 355^\circ$	$35^\circ \sim 65^\circ$	15	NLOS
	2		$-5^\circ \sim 25^\circ$	82.96	NLOS
	3		$-5^\circ \sim 25^\circ$	82.67	NLOS
	4		$5^\circ \sim 35^\circ$	27.66	NLOS
	5		$-5^\circ \sim 25^\circ$	86.12	LOS
	6		$-5^\circ \sim 25^\circ$	81.99	LOS
	7		$5^\circ \sim 35^\circ$	34.42	LOS
	8		$-5^\circ \sim 25^\circ$	100.8	LOS
	9		$-5^\circ \sim 25^\circ$	56.58	LOS
	10		$-5^\circ \sim 25^\circ$	164.49	LOS
	11		$-5^\circ \sim 25^\circ$	81.94	NLOS
	12		$-5^\circ \sim 25^\circ$	84.11	NLOS
	13		$15^\circ \sim 45^\circ$	24.43	NLOS
Tx		$0^\circ \sim 355^\circ$	$-20^\circ \sim 10^\circ$		

TABLE II
THE SPECIFICS OF $\sigma_{SF}(dB)$

	LOS							**NLOS**		
Routes	**route 1**				**route 2**			**route 3**		
Obstacle size (m)	100	50	20	10	50	20	10	50	20	10
mean of $\sigma_{SF}(dB)$	1.93	1.83	1.63	1.38	2.13	1.36	1.14	3.95	3.09	2.61
min of $\sigma_{SF}(dB)$	1.71	1.46	0.91	0.72	1.83	0.71	0.51	3.25	2.22	0.72
max of $\sigma_{SF}(dB)$	2.72	3.49	4.35	2.49	3.41	2.84	3.20	4.88	4.44	4.59
3GPP-TR 38.900 $\sigma_{SF}(dB)$	4.0							7.82		

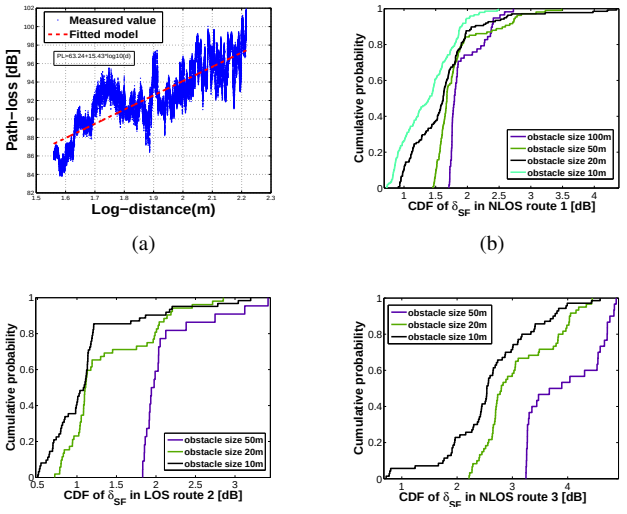

(a) (b) (c) (d)

Fig. 4. (a)The example of linear fitted model, (b)CDF of μ_{SF} in route 1 (LOS), (c)CDF of μ_{SF} in route 1 (LOS), (d)CDF of μ_{SF} in route 1 (NLOS)

where the N is the number of the measured points in the scope of obstacle size. It is the obstacle that caused the shadow fading. The μ_{PL} is the value of actual pathloss . It can be calculated by the linear fitted model (shown in Fig. 4(a)) according to a given Tx-Rx distance. Due to the much more serious propagation attenuation compared with the frequency below 6 GHz, the mmWave is more likely be be used to cover micro cell with radius about 30 m to 300 m. So when investigating the shadow fading, smaller size obstacles need to be considered. Here we calculate the σ_{SF} of different obstacle size of 10 m, 20 m, 50 m and 100 m for getting more reliable results.

Traditionally, the pathloss is modeled by mingling measured data of different routes from one cell or different cells for increasing the applicability of the model. However, this may decrease precision of the model when it is applied to a specific environment due to the difference of different measured routes. The σ_{SF} can be overestimated and [7] has conformed this based ray-tracing result. Here, the σ_{SF} is calculated with data from each single route. This means there are different results in all the measured routes. The specific values of the σ_{SF} in each route are listed in the table II. The cumulative distribution function (CDF) of σ_{SF} in each route are shown in Fig. 4(b-d). The different colors represent the different results when considering different obstacle size. Four different kinds of obstacle size are considered in route 1 while three kinds of obstacle size are considered in route 2 and route 3 because of the limited Tx-Rx distance. We do not calculated the result of σ_{SF} with traditional method because of the limited measured routes. The values in standard Recommendation [13] are adopted as the typical results of traditional method.

We adopt the mean of σ_{SF} of the calculated results in each route as the reference here. It is obvious that the σ_{SF} calculated by data in a single route is much less than the value

adopted in standard Recommendation [13]. The true value of σ_{SF} is just about half of the value in [13]. in the LOS routes. In the NLOS routes, the σ_{SF} that we calculated is just about two thirds of the value in [13].

IV. 3-Dimensional Angle Domain

The knowledge of angle domain is very important for better application of this frequency band. This section study the angle characteristics based on the data from (HAB) measurement. With the SAGE estimation algorithm introduced in [8], the needed parameters to characterize the channel can be extract. The number of estimated multi-path component (MPC) is set to be 100 which is large enough to capture all the significant power. Then the synthetical CIR h can be represented as

$$h = \sum_{l=1}^{L} ||\alpha_l|| A_l(\psi)\delta(\tau - \tau_l) \tag{5}$$

where the $||\alpha_l||$, τ_l and $A_l(\psi)$ represent the modulus of amplitude response, delay and angle of each path respectively. The parameter $\psi = [\phi, \theta]$ contains the azimuth angle and the elevation angle.

A. RMS angular spread

The RMS azimuth angle spread can be calculated by

$$\sigma_{AS} = \sqrt{\frac{\sum_{l=1}^{L}(\psi_l - \mu_\psi)^2 P_l}{\sum_{l=1}^{L} P_l}} \tag{6}$$

where the ψ refers to the angle information (AOA or AOD) of each path. The AOA and AOD are estimated with data in step 1 and data in step 2 of HAB measurement separately. P_l is square of the amplitude response of each path. The μ_ψ can be obtained by

$$\mu_\psi = \frac{\sum_{l=1}^{L} \phi_l P_l}{\sum_{l=1}^{L} P_l} \tag{7}$$

The calculated results are listed in table III, including (AASA), (EASA), (AASD) and (EASD). We averaged the results in LOS and NLOS environment separately. By comparing the measured results with the value in standard Recommendation [13] shown in table III, we can see the AASA match well with the Recommendation and the AASD is slightly bigger than the recommendation. This may due to tall building near the Tx caused richer reflectors as shown in 2(a). For investigating the relationship between azimuth angle with Tx-Rx distance and specific environment, we plot the distance characteristics of ASA and ASD in different environments.

Fig. 5(a) shows the AASA of the six LOS measured sites. The AASA clearly descends with the Tx-Rx distance except the site Rx-6. It is because there are face-to-face reflectors in the site Rx-6 from the view of Tx while other sites do not have this condition. In NLOS enviroment, the AASA is much related to the specific environment. As shown in Fig. 5(b), we can clearly see that the seven NLOS measurement sites can be divided into 3 groups (A, B, C). The sites Rx-1,RX-4 and Rx-13 (group A) are relative closer to the Tx and the mean AASA of them is $68°$. The other four NLOS sites are far away from the Tx, however the AASA of Rx-3 and Rx-11 (group B) are obviously larger than that value of Rx-2 and Rx-12 (group C). It is because that there are reflectors in sites Tx-3 and Tx-11 and the two sites are near the border of LOS and NLOS environment. The mean value of group B and group C are $114°$ and $20.5°$ respectively.

The AASD of LOS sites are shown in Fig. 5(c). The six LOS measured sites can be classified into 2 groups as well. The mean AASD of the two groups are $86.9°$ and $13.1°$ respectively. The difference between the sites in the two groups lies in that if there is valid reflectors in the Tx from the view of Rx sites. This can account for the big gap between the mean AASD of the two group Rx sites. The Fig. 5(c) shows the AASD of the 7 NLOS measured sites, we can find the sites in group B which has further Tx-Rx distance has much smaller AASD than the sites in group A which is much closer to the Tx. The mean AASD of the two group are $105.1°$ and $17.3°$ respectively.

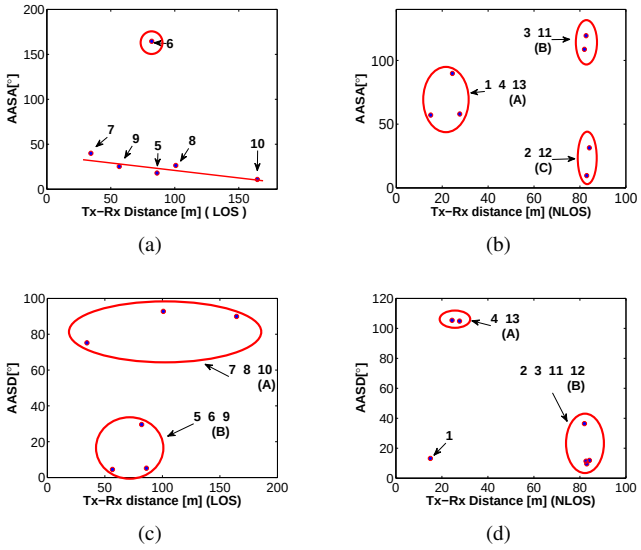

Fig. 5. (a)AASA in NLOS sites, (b)AASA in LOS sites, (c)AASD in NLOS sites, (d)EASD in NLOS sites

B. Cluster characteristics

The KPowerMeans algorithm which is introduced in [12] is adopted to get the cluster results of each measured site with the angle information both in azimuth and elevation. Due to the AOA and AOD of the paths were not obtained synchronous in the HAB measurement, the estimated paths in step 1 and step 2 of the measurement can not be one-to-one corresponded. So the clustering result of paths in step 1 (CP1) just can be calculated with parameter space $P1$

$$P1 = (AOA, \tau) \tag{8}$$

TABLE III
THE SPECIFICS OF ANGLE DOMAIN

Sites	AASA [°]	EASA [°]	AASD [°]	EASD [°]	number of CP1	number of CP2	Environment
1	57.1	6.7	13.2	9.8	2.0	13.7	NLOS
2	9.6	7.1	9.5	7.8	10.1	12.1	NLOS
3	119.4	5.9	11.4	4.4	4.8	11.0	NLOS
4	58.0	7.7	104.8	6.04	14.2	16.3	NLOS
5	18.0	7.6	5.1	4.7	9.5	11.4	LOS
6	164.52	3.5	29.6	5.0	2.1	2.0	LOS
7	40.0	8.4	75.2	6.3	14.0	14.5	LOS
8	26.4	9.8	92.8	5.0	7.3	10.2	LOS
9	25.3	10.2	4.5	10.8	13.7	6.0	LOS
10	10.9	7.4	90.0	3.8	4.3	10.5	LOS
11	108.7	4.5	36.4	5.7	2.2	2.4	NLOS
12	31.4	6.9	11.9	5.1	2.4	8.9	NLOS
13	89.8	8.4	105.4	5.4	12.5	16.3	NLOS

TABLE IV
COMPARISON WITH STANDARD RECOMMENDATION

	Angle Spread (log10[°])				Cluster number			Inner Cluster AS [°]			
	Measurement		3GPP		Measurement		3GPP	CP1-AASA	CP2-AASD	3GPP	
c	AASA	AASD	AASA	AASD	CP1	CP2				AASA	AASD
LOS	1.48	1.43	1.61	1.28	8.5	9.1	12	6.48	3.3	17	3
NLOS	1.71	1.40	1.69	1.19	7.5	11.5	19	10.62	4.62	22	10

while the clustering result of paths in step 2 (CP2) just can be calculated with parameter space $P2$

$$P2 = (AOD, \tau) \tag{9}$$

Both the AOA and AOD include the azimuth angle and elevation angle. We captured data of 100 cycles in every rotation step. The mean cluster number of the 100 cycles is adopted. Figure 6 and figure 7 show an example of the clustering result of site 8. Different clusters are marked in different colors. The specific value of all the 13 sites are shown in table III. As we can see, the number of CP2 is generally greater than the number of CP1 except the Tx-11 site. Table IV shows the mean measurement results versus standard Recommendation. The mean numbers of CP1 in LOS and NLOS environments are 8.5 and 7.5 respectively. Meanwhile, the mean numbers of CP2 in LOS and NLOS environments are 9.1 and 11.5 respectively. Both the numbers of CP1 and CP2 are obviously less than the adopted value in standard Recommendation [13]. This means the number of the clusters will be much smaller when the parameter space of clustering algorithm lacks AOA or AOD.

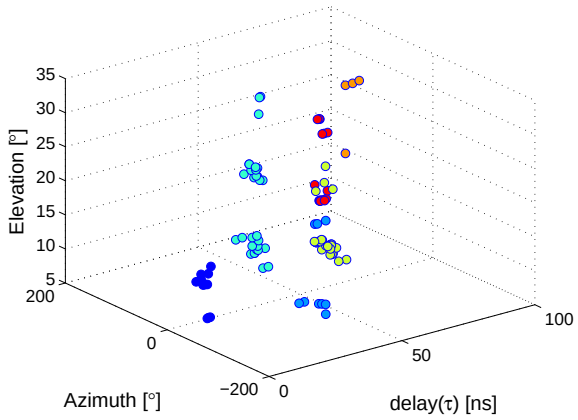

Fig. 6. the cluster result of site 8 (CP1)

V. CONCLUSION

In this paper, we study the wideband channel characteristics of 28 GHz in UMi scenario based the measurement in Beijing. Both the shadow fading and 3-Dimensional angle information of the recognizable paths are studied. Different from the traditional statistical method, we calculated the σ_{SF} with data captured in each single route instead of the mingled data from different routes. It is found that the σ_{SF} in specific environment is much less the value in standard Recommendation [13]. The real σ_{SF} that we calculated in each LOS route is just about half of the value adopted in [13]. Meanwhile, in the NLOS route,the σ_{SF} is just about two thirds of the value in [13]. In addition, we studied the AASA, EASA, AASD and EASD in each of the 13 sites based on rotation measurement. The specific values are given and are analysed with the propagation environment in each site. The cluster characteristics is also investigated. Both the clustering result calculated with parameter space $P1(AOA, \tau)$ and the clustering result calculated with parameter space $P2(AOD, \tau)$ are given and compared. It is found the cluster number is bigger when choosing $P2(AOD, \tau)$ as parameter space of clustering algorithm. However, when comparing with the value

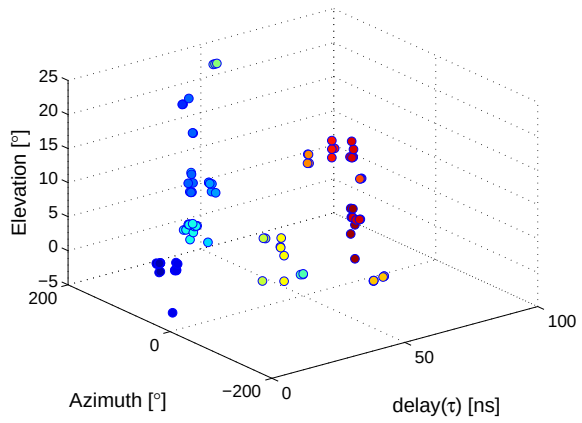

Fig. 7. the cluster result of site 8 (CP2)

in standard Recommendation [13], both the two results are much smaller. This means the cluster number of the result will be much smaller when the parameter space of clustering algorithm lacks AOA or AOD.

ACKNOWLEDGMENT

The research is supported in part by National Natural Science Foundation of China and project name is "Theoretical Modeling and Experiment Research of Propagation Channel"with NO. 61322110, and in part by National Science and Technology Major Project of the Ministry of Science and Technology and project name is "IMT-2020 Candidate Band Analysis and Evaluation" with 2015ZX03002008, and in part by Zhongxing Telecommunication Equipment Corporation.

REFERENCES

[1] J. H. Zhang, P. Tang, and L. Tian, "The current and future of high frequency channel modeling," *in Telecommunication Network Technology*, vol. 2016, pp. 10¨C17, 2016.

[2] METIS, Mobile and wireless communications Enablers for the Twentytwenty Information Society, *D1.2, Initial channel models based on measurements*, [Online]. Available: http://www.metis2020.com.

[3] Y. Azar, G. N. Wong and K. Wang, "28 GHz propagation measurements for outdoor cellular communications using steerable beam antennas in New York city," *2013 IEEE International Conference on Communications (ICC)*, pp. 5143-5147, June. 2016.

[4] S. Hur, Y. J. Cho and Taehwan Kim, "Wideband spatial channel model in an urban cellular environments at 28 GHz," *2015 9th European Conference on Antennas and Propagation (EuCAP)*, pp. 1-5, May. 2015.

[5] M. Samimi, K. Wang and T. S. Rappaport, "28 GHz Angle of Arrival and Angle of Departure Analysis for Outdoor Cellular Communications Using Steerable Beam Antennas in New York City," *2013 IEEE 77th Vehicular Technology Conference (VTC Spring)*, pp. 1-6, June. 2013.

[6] G. R. MacCartney, M. K. Samimi and T. S. Rappaport, "Omnidirectional path loss models in New York City at 28 GHz and 73 GHz," *2014 IEEE 25th Annual International Symposium on Personal, Indoor, and Mobile Radio Communication (PIMRC)*, pp. 227-231, Sept. 2014.

[7] A. F. Molisch, A. Karttunen and S. Hur, "Spatially consistent pathloss modeling for millimeter-wave channels in urban environments," *2016 10th European Conference on Antennas and Propagation (EuCAP)*, pp. 1-5, April, 2016.

[8] B. H. Fleury, M. Tschudin and R. Heddergott, "Channel Parameter Estimation in Mobile Radio Environments Using the SAGE Algorithm," *IEEE Journal on Selected Areas in Communications*, vol. 17, pp. 434¨C450, Mar 1999.

[9] V. Erceg, L. J. Greenstein and S. Y. Tjandra "An empirically based path loss model for wireless channels in suburban environments," *IEEE Journal on Selected Areas in Communications*, vol. 17, N. 7, pp. 1205-1211, Jul. 1999.

[10] X. Wu, C. X. Wang and J. Sun, "60 GHz Millimeter-Wave Channel Measurements and Modeling for Indoor Office Environments," *IEEE Transactions on Antennas and Propagation*, vol. PP, no. 99, pp. 1-1, 2017.

[11] Tao Jiang, Lei Tian and Jianhua Zhang, "Basestation 3-Dimensional Spatial Propagation Characteristics in Urban Microcell at 28 GHz," *European Conference on Antennas and Propagation (EuCAP)*, 2017 IEEE, 11th, Paris, 2017(A).

[12] N. Czink, P. Cera and J. Salo "A Framework for Automatic Clustering of Parametric MIMO Channel Data Including Path Powers," *IEEE Vehicular Technology Conference*, pp. 1-5, Sept. 2006.

[13] 3GPP TR 38.900 V2.0.0, "Channel model for frequency spectrum above 6 GHz," Technical Report, June. 2016.